IOSR Journal of Applied Geology and Geophysics (IOSR-JAGG)
e-ISSN: 2321–0990, p-ISSN: 2321–0982.Volume 9, Issue 4 Ser. I (Jul. – Aug. 2021), PP 47-66
www.iosrjournals.org

Structural framework of the southern offshore region of the Gulf of Suez as deduced from gravity data

Saada Ahmed Saada[1], Alaa Mustafa Badr[1,3,*], Ramadan Abdallah El Gezeery[2]
[1]*Geology Department, Faculty of Science, Suez University*
[2]*Geology Department, Faculty of Science, Zagazig University*
[3]*Suez Oil Processing Company (SOPC), Suez, Egypt*
**Corresponding author: Ali.Maged@suezuni.edu.eg*

Abstract:
The study area covers the southern offshore portion within the Gulf of Suez (GS) with a surface area of about 4000 km^2. The present work aims to evaluate and outline the subsurface geologic conditions and structural framework controlling the study area. To achieve this aim, subsurface geophysical techniques were carried out on Bouguer gravity map. They indicate that the GS is formed from alternative positive and negative anomalies trending mainly in the NW directions. Sharp positive gravity anomalies are located mainly on the eastern and western shoulders while board negative ones are concentrated at the middle parts. Depth estimation methods were applied to locate the depth to basement rocks, which ranges from 1.5 km at the eastern and western areas to about 5.5 km at the central parts. Also tilt angle derivative (TD) was applied to gravity data to locate the edges of gravity sources. A tentative basement structural map was constructed from the filtered gravity maps. This study indicates that the area is formed from up-lifted and down-faulted blocks intersected by transform faults with NNE to NE direction. Two and half dimension (2.5-D) gravity modeling in the NE direction was applied to confirm and adjust the proposed basement structures and to give more information about the causative bodies. Finally, a tentative basement depth map was constructed to throw more light on thickness variation of the sedimentary cover. It shows a maximum thickness within the middle part and decreases to the coastal areas.

Key Word*: Gulf of Suez; gravity; geologic structure; data analysis.*

Date of Submission: 28-06-2021 Date of Acceptance: 12-07-2021

I. Introduction

The GS basin has an elongated depression trending in the northwest direction and separating Sinai Peninsula and the Eastern Desert-Red Sea mountains. The average distance between these shield masses is about 85km. It is 320 km long and has a width varies from 30 - 80 km (Figure 1). The water depth of GS is relatively shallow (average depth is about 65m) compared to Gulf of Aqaba (attains a depth of about 2000m in some parts). The central one-third of the GS rift basin is occupied by water, while the other two thirds are exposed onshore [1]. The rift basin is bounded from both sides by two major marginal fault systems, which are characterized by lines of high vertical escarpments on the up thrown sides [2].

Because of the importance of the GS as the main oil-producing province in Egypt, numerous investigations, and discussions since more than sixty years ago are carried out. Many authors have undertaken its geology, stratigraphy, tectonics, and geological history.

In this work, the authors try to throw more light on the structural framework using the Bouguer gravity map and some drilled wells within the investigated area. Therefore, different analytical techniques were applied to achieve this goal.

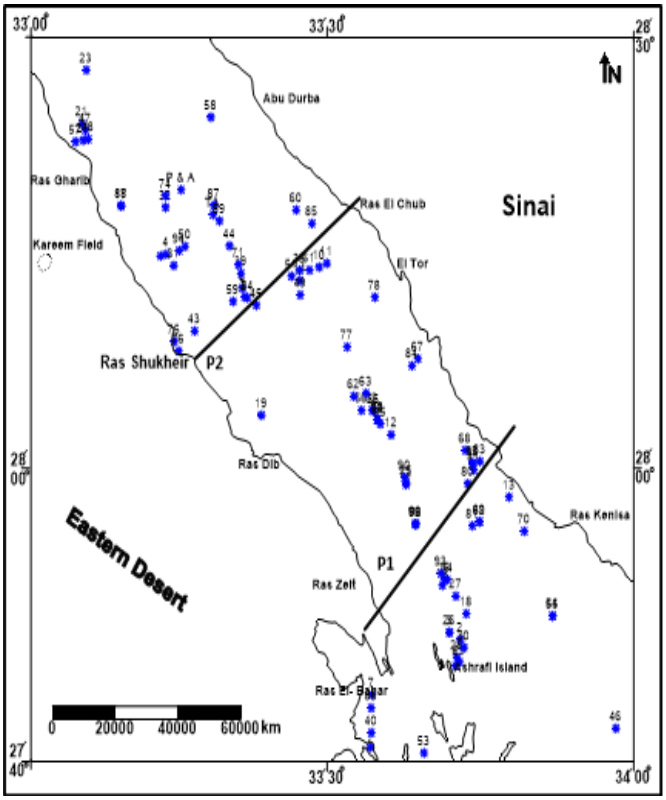

Figure (1): Location map shows the oil drilled well and the modelled profiles of the study area.

Geologic Setting

Subsurface Stratigraphy

The stratigraphic sequence of the area, as deduced from different drilled wells ranges in age from the Permo-Carboniferous (Nubia C) to the Recent (Figure 2). This sequence is unconformably overlying the basement rocks, and it is variable in thickness from one place to another. The GS involves a series of parallel half -grabens with thick Miocene and Post-Miocene sediments. Major faults at the shoulder and inside the GS basin are of NNW-SSE trend. These faults are composed mainly of complex pattern of Suez and Aqaba trends and the crossing among these trends are common. In the eastern side of the GS, major Clysmic faults are cut obliquely by major faults of Gulf of Aqaba direction. In the western side, the trend of Aqaba is common, but important cross faults trending NE - SW are present. Such cross faults delineate most of the Pre-Miocene oil fields, as Ras Gharib, Bakr and Amer [3].

Folding plays a minor role in controlling the structural pattern of the GS. Most of the noticed folds were either produced by bending of the strata before breaking or by movements caused the less rigid sediments, especially the Miocene sediments, to bend in anticlinal or synclinal folds [2]. Some of these pseudo-anticlines may have developed as a consequence of movements on large scale wrench faults.

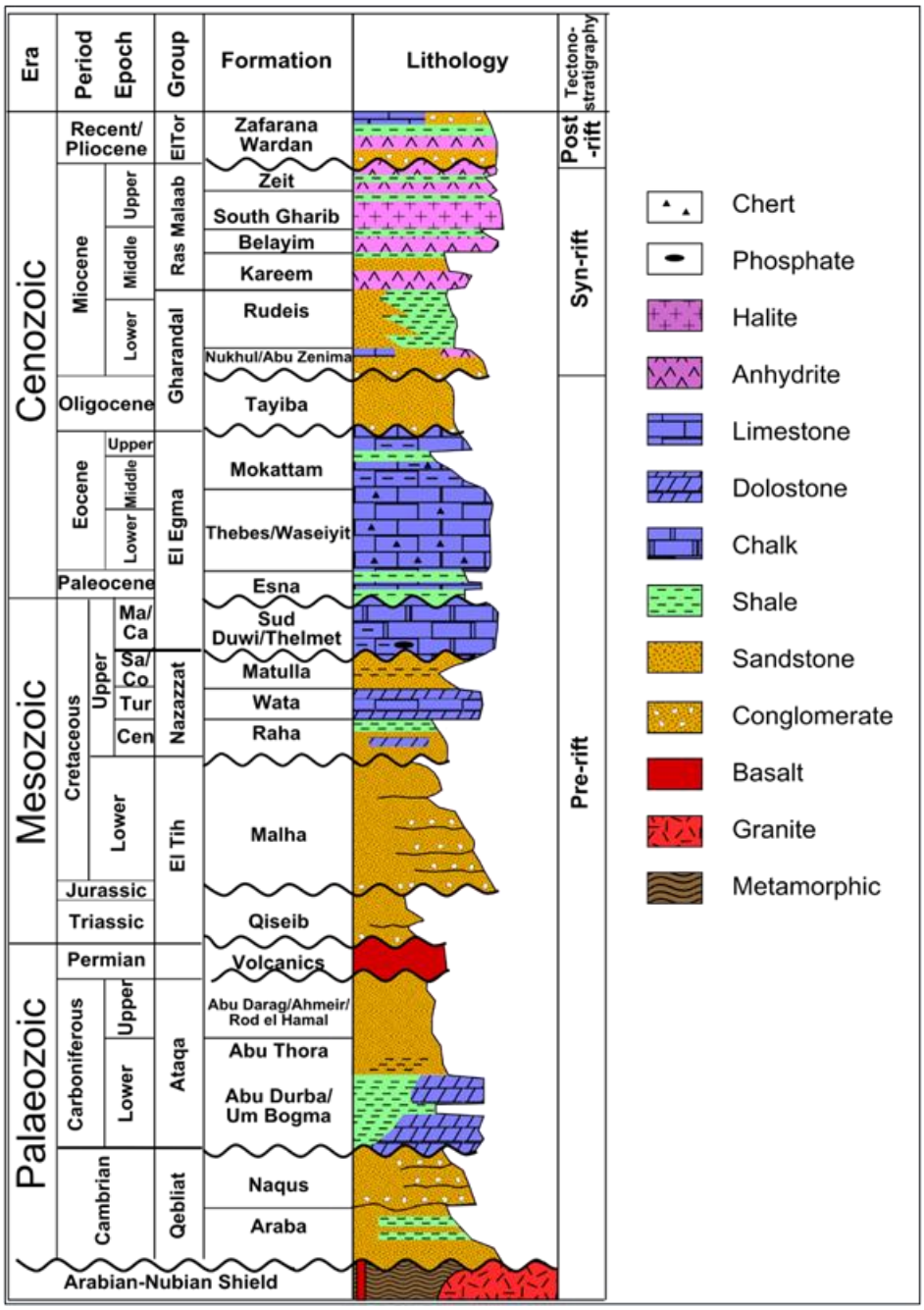

Figure (2): Stratigraphy and succession of pre-Miocene at the GS rift modified after [4].

Tectonics

Tectonically, Moustafa [5] divided the GS into three provinces depending on the dip regime direction for each province. He named these provinces from North to South as; Wadi Araba, Belayim and Amal provinces. The first one (Wadi Araba province) is separated from Belayim one by the Galala - Zenima hinge zone, while Morgan hinge zone separates Belayim and Amal provinces. The Galala – Zenima and Amal hinge zones are trending in the NE-SW direction. The dip contrasts exist as follows: The northern Araba and the southern Amal provinces exhibit a SW dip, while the central Belayim province shows a NE dip. Moustafa [6] concluded that the alternating distribution of parent rocks and conduits of transport of rift sediments together, which the incipient half graben geometry of the GS have created sediments wedges of opposing thickness attitudes, thus creating the three dip provinces of the GS. Net rotation of the dip provinces took place along the two-accommodation zones, the northern one is named Zaafarana accommodation zone, while the southern one is named Morgan accommodation zone (Figure 3).

Colletta et al. [7] showed that, the polarity of the tilted blocks changes twice along the longitudinal extension of the GS rift. Therefore, three provinces stretching on average of 50-100 km are identified: in the

northern part, the Darag basin was tilted to the southwest, in the central part, the Belayim province was tilted to the northeast, and to the south, the Amal - Zeit province was tilted to the southwest. Moreover, the values of the tilting angles are differing from one province to another. The following values have been recorded, 5□ - 10□ in the Darag basins, 20 - 25□ in the Amal-Zeit province. In the Syn-rift system, the tilting angle seldom exceeds 10□.

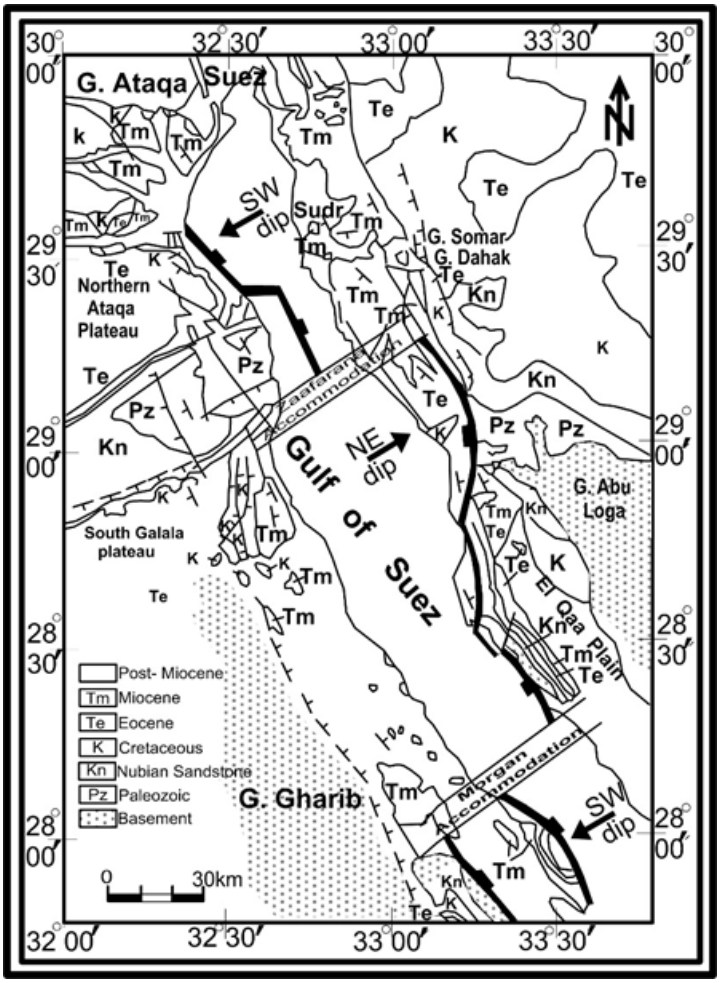

Figure (3): Three tectonic provinces of the GS (After [6])

Many authors [8-11] suggested that the Gulf of Suez is structurally divided into four tectonic provinces (I, II, III and IV) as illustrated in Figure (4). These provinces are separated by three tectonic lines (Alfa, Beta and Gamma) and considered as major transform faults, trending parallel to the trend of Aqaba (NNE - SSW). These faults resulted from a partial movement of Sinai relative to Africa. These three fault lines extend from Ras Zaafarana, Ras Shukheir, and Gemsa. The four provinces form two lows (Abu Zeneima and Hurghada basins), alternating with two structural highs (Ayun Musa and Araba - Zeit blocks). The first and the third provinces are uplifted blocks while the second and fourth provinces are down faulted blocks.

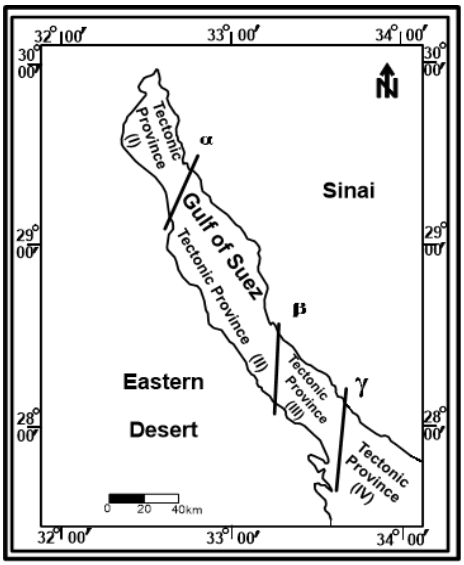

Figure Error! No text of specified style in document.**(4):** The four tectonic provinces of the GS (after [8]).

II. Data And Methodology

This work is based mainly on the Bouguer gravity anomaly map (Figure 5) of the study area. It was provided by the Egyptian General Petroleum Cooperation [12] with a scale of 1:250,000 and contour interval of 0.5 mGal. Eighty-four basement drilled wells are used to constrain the modeled profiles and the basement relief map.

The separation of regional and residual component was applied to throw more light on the main structural blocks that were formed within the offshore area. The trend analysis was applied to Bouguer, low-pass and high-pass maps to reveal the geologic history of the investigated area. Depth to basement rocks was applied to determine the average thickness of the sedimentary cover. Tilt angle derivative was used to outline the edges of the uplifted and downfaulted blocks. From the integration of these methods the structure map of the area can be deduced. The available drilled wells were utilized to constrain the modeled profiles. Finally, a basement relief map can be constructed.

III. Result

Analysis and interpretation of gravity data

Qualitative interpretation of Bouguer anomaly map:

The Bouguer map (Figure 5) shows that the considered area is characterized by negative anomalies with low frequencies in the offshore parts. The minimum amplitude lies in the northern offshore part between Ras Gharib and Abu Durba and attains about -20 mGal. The positive anomalies are concentrated along the shoreline and characterized by sharp and high frequencies with amplitudes range from 2 to 41 mGals. The gravity anomalies trend mainly in the NW-SE direction parallel to the shorelines.

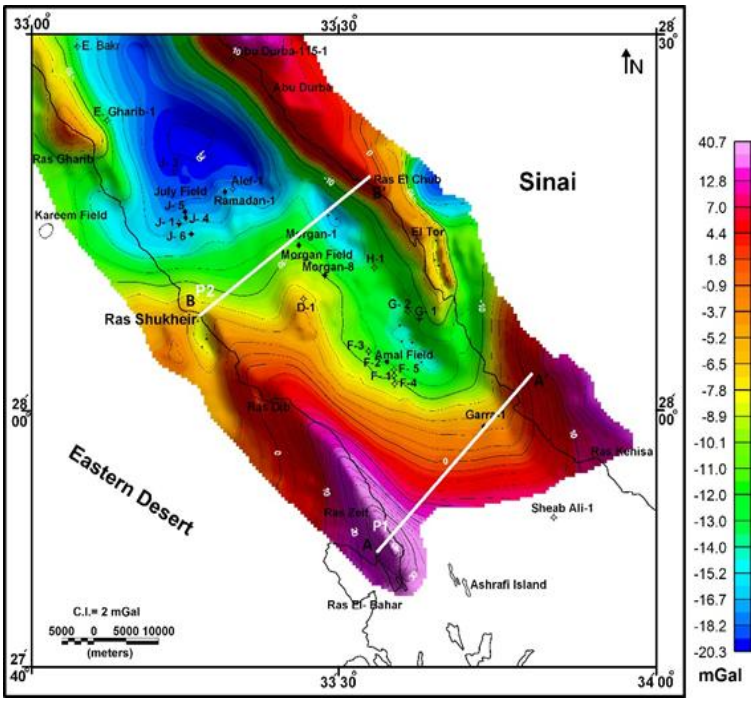

Figure (5): Bouguer map (after the EGPC,1984) displays the location of the modeled profiles.

Regional -residual separation of gravity data

The potential anomaly measured at the surface is not produced by one simple structure, but it is the sum of the effects of a number of subsurface structures buried at different depths. The separation process is used to isolate the anomalies caused by shallower geologic features from those of deeper ones. By removing the regional field from the observed one; the residual field is obtained. Generally, the regional anomalies are considered broad and smoothed; they are associated with the deep and larger structures, while the residual ones seem to be of sharp and high frequency, which reflect the shallow bodies [13]. So, the residual anomalies can be demarcated as the unconventionality from the mean or regional surface. The isolated residual components are significant to focus any shallow geologic features that are generally of highest awareness in the geological prospecting.

Bouguer maps is subjected to filtration process by using the low-pass and high-pass filtering operators by using frequency domain [14]. They have been mainly established for separating regional and residual components. Those two techniques depend on frequency or wavelength or both of the transformed anomaly.

The relationship between the depth of a source and its wavelength is exploited to enhance the appearance of sources from specific depths by low-pass and high-pass filtering. So, high-pass filtering decreases the appearance of deep sources and conversely, low pass filtering tends to reduce the appearance of shallow sources [15].

Figure (6) shows the radial average pwer spectrum of Bouguer gravity data. The curve shows the deep (regional) and shallow (residual) sources that are characterized by small and high wavenumbers, respectively. In addition, the examination of the resulted radially averaged log power spectrum shows that a lower wavenumber one (regional component) less than 0.02 Rad/m (about 7 km depth) demonstrates the deep-seated geologic features (structures and/or intrusions). Meanwhile, higher wavenumbers denote the shallow geologic features. Spectral analysis gives an averaging depth estimated from the radial power spectrum. The power spectrum chart of a gravity field usually involves two segments that approximate to straight lines (regional and residual components); the slope is the function of the depth of the accumulation of sources [16].

The low-pass (regional) gravity map Figure (7) reveals strong, clear, deep and wide-ranging anomalies that extends all over the southern part of the Gulf. This map has high amplitudes and long wavelength. The gravity values range from -22.2 mgal to +30 mGal. The map clarifies the major trends affecting the deep-settled structures, which takes place in the NW and NE trend.

The high-pass (residual) gravity map (Figure 8) displays anomalies that are originated from shallow gravity sources. This map reflects alternated positive and negative anomalies with low amplitudes and short wavelengths. Both anomalies have a NW direction. The residual field, as shown in Figure (8), ranges from -9.9 mgal to +12.5 mGal. The local variations in both wavelengths and amplitudes of these anomalies may be due to the difference in the compositions and/or relative depths of their sources.

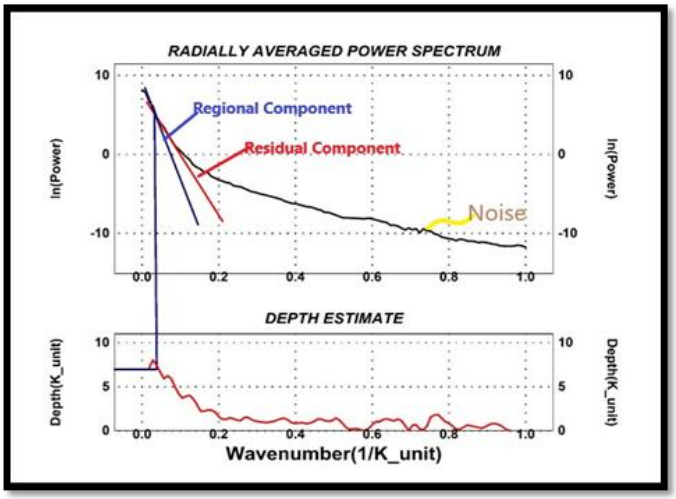

Figure (6): Gravity power spectrum shows the regional and residual components.

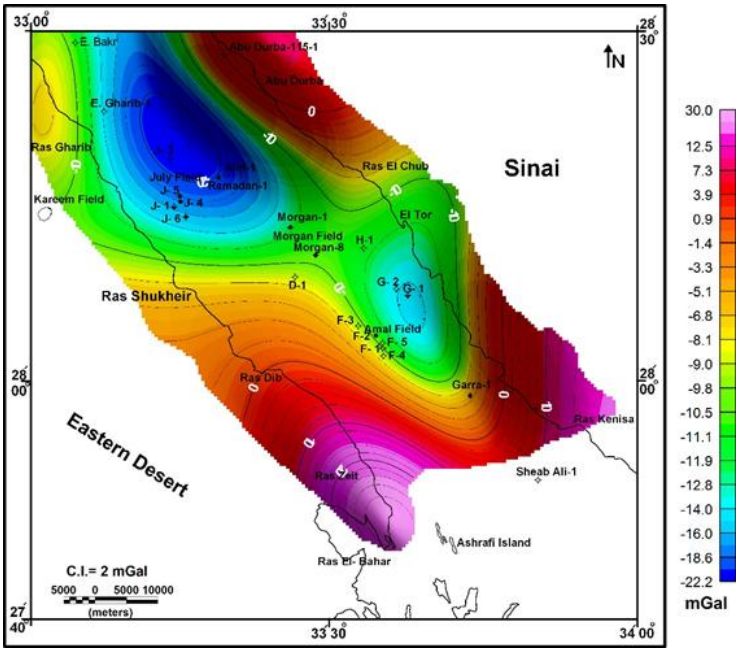

Figure (7): Low pass (regional) filter of Bouguer gravity map.

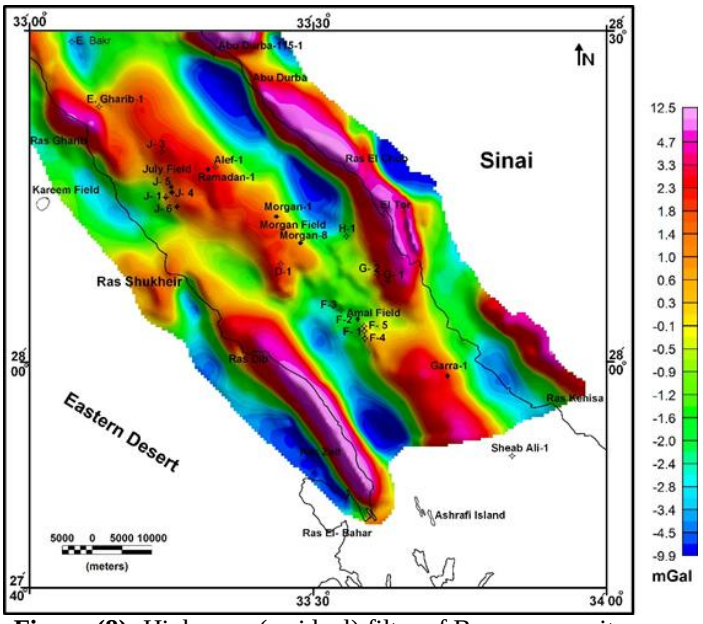

Figure (8): High-pass (residual) filter of Bouguer gravity map.

Trend analysis

Trend analysis is one of the most important elements in quantitative interpretation. The main purpose this technique is to define statistically the tectonic trends developed in the area. It may help in the study of the tectonic forces, which affected the basement rocks and the overlaying sedimentary cover. The trend analysis is a method by which the tectonic setting of the area is determined, where tectonic history of the rocks is in some degree recorded from the magnitude and pattern of gravity anomalies [17].

The gravity trends are applied to the Bouguer, lowpass, and highpass gravity maps using Affleck's [17] technique. The results of lineament analysis are illustrated in tables 1-3. They show five tectonic trends, namely: GS (N35°-45°W) trend East African (N-S) trend, Najd (N65°W) trend, Aqaba (N15°-25°E) trend, Mediterranean (E-W) trend and arranged in a decreasing order of abundance. For visual inspection, Figure (9) shows these trends in a frequency diagram.

Table (1): Parameters of the major trends detected from Bouguer gravity map.

WEST					Azimuth	EAST				
N	N%	L	L%	L/N		L/N	L%	L	N%	N
3.0	10.0	24718.0	6.2	8239.3	0:<10	11212.3	8.5	33637.0	10.0	3.0
3.0	10.0	35227.4	8.9	11742.5	10:<20	14721.5	3.7	14721.5	3.3	1.0
2.0	6.7	20784.6	5.2	10392.3	20:<30	14313.2	3.6	14313.2	3.3	1.0
5.0	16.7	86884.2	21.8	17376.8	30:<40	-	0.0	0.0	0.0	0.0
6.0	20.0	113775.2	28.6	18962.5	40:<50	-	0.0	0.0	0.0	0.0
2.0	6.7	19177.6	4.8	9588.8	50:<60	-	0.0	0.0	0.0	0.0
3.0	10.0	25623.7	6.4	8541.2	60:<70	-	0.0	0.0	0.0	0.0
1.0	3.3	9122.9	2.3	9122.9	70:<80	-	0.0	0.0	0.0	0.0
0.0	0.0	0.0	0.0	-	80:<90	-	0.0	0.0	0.0	0.0
25.0	83.3	335313.7	84.3		Sum		15.7	62671.6	16.7	5.0
∑n	30.0		∑L	397985.3		∑n%	100.0		∑L%	100.0

Table (2): Parameters of the major trends detected from regional gravity map.

WEST					Azimuth	EAST				
N	N%	L	L%	L/N		L/N	L%	L	N%	N
3.0	17.6	54851.5	19.5	18283.8	0:<10	16854.5	6.0	16854.5	5.9	1.0
1.0	5.9	7701.8	2.7	7701.8	10:<20	14405.0	5.1	14405.0	5.9	1.0
2.0	11.8	14876.3	5.3	7438.1	20:<30	12132.1	4.3	12132.1	5.9	1.0
2.0	11.8	54987.7	19.6	27493.9	30:<40	-	0.0	0.0	0.0	0.0

3.0	17.6	44240.2	15.8	14746.7	40:<50	-	0.0	0.0	0.0	0.0
1.0	5.9	22704.5	8.1	22704.5	50:<60	14424.7	5.1	14424.7	5.9	1.0
1.0	5.9	23491.6	8.4	23491.6	60:<70	-	0.0	0.0	0.0	0.0
0.0	0.0	0.0	0.0	-	70:<80	-	0.0	0.0	0.0	0.0
0.0	0.0	0.0	0.0	-	80:<90	-	0.0	0.0	0.0	0.0
13.0	76.5	222853.5	79.4		Sum		20.6	57816.2	23.5	4.0
∑n	17.0		∑L	280669.7		∑n%	100.0		∑L%	100.0

Table (3): Parameters of the major trends detected from residual gravity map.

WEST					Azimuth	EAST				
N	N%	L	L%	L/N		L/N	L%	L	N%	N
2.0	3.6	24425.7	3.5	12212.9	0:<10	6774.1	1.9	13548.2	3.6	2.0
6.0	10.9	72478.4	10.4	12079.7	10:<20	-	0.0	0.0	0.0	0.0
6.0	10.9	53250.0	7.6	8875.0	20:<30	2973.6	2.6	17841.9	3.6	6.0
14.0	25.5	227401.2	32.6	16242.9	30:<40	509.3	1.0	7130.7	1.8	14.0
7.0	12.7	117012.2	16.8	16716.0	40:<50	1024.8	1.0	7173.4	1.8	7.0
6.0	10.9	88130.3	12.6	14688.4	50:<60	0.0	0.0	0.0	0.0	6.0
4.0	7.3	34530.8	4.9	8632.7	60:<70	0.0	0.0	0.0	0.0	4.0
0.0	0.0	0.0	0.0	-	70:<80	-	1.1	7540.1	1.8	0.0
1.0	1.8	9475.7	1.4	9475.7	80:<90	17847.2	2.6	17847.2	3.6	1.0
46.0	83.6	626704.2	89.8		Sum		10.2	71081.6	16.4	40.0
∑n	86.0		∑L	697785.8		∑n%	100.0		∑L%	100.0

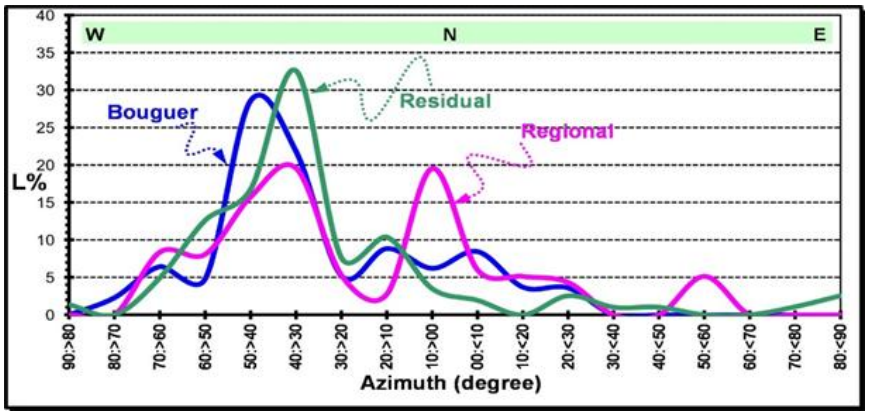

Figure(Error! No text of specified style in document.**):** Frequency distribution curves of the gravity tectonic trends.

Maps / Orders	Bouguer trends	Low-pass trends	Low-pass trends
1St order	Suez	Suez	Suez
2nd order	E. Africa	E. Africa	Najd
3rd order	Najd	Najd	E. Africa
4th order	Aqaba	Aqaba	Tethyan
5th order	-	Syrian	Aqaba
6th order	-		Tibesti

Depth estimation methods

Gravitational field measurements are utilized in exploration geophysics to investigate the subsurface distributions and depths of different geologic features. The measurements require a number of corrections to improve the expression of local field variations. These corrections are applied to produce clean and robust output suitable for interpretation [18]. Potential field methods (gravity and magnetic) have been widely used to calculate the depth to basement rocks because sediments are usually found with low density and were weakly magnetized. The basement rocks are characterized by higher density than the overlaying sedimentary rocks. In this situation, regional gravity and magnetic anomaly can be attributed to variations in the depth to basement [19].

In our study, the depth to causative bodies is calculated using spectral analysis technique along twenty gravity profiles chosen on the Bouguer gravity map. These profiles are clearly illustrated and located in Figure 10.

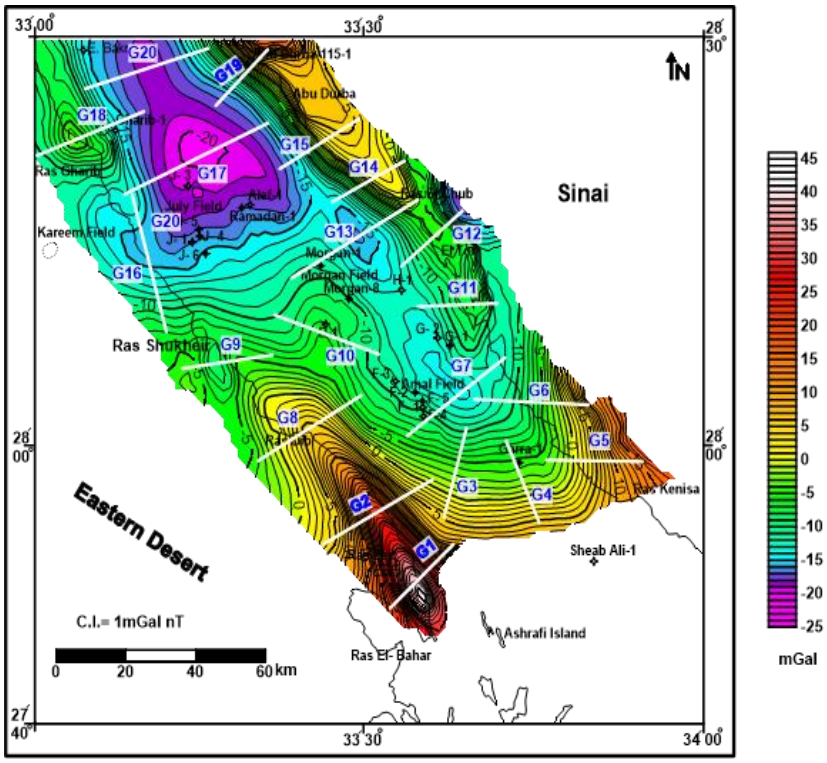

Figure (10): Bouguer map shows the locations of gravity spectral analysis profiles (G1-G20).

The results of depth estimation supply information concerning with the thickness of the sedimentary succession. Consequently, it is possible to delineate the configuration of the sedimentary basins in the study area and give an idea about the topography of deeply buried basement. Figure (11) illustrate an example for the spectral analysis calculation along profile G12, using, [16], method. All the results of spectral analysis technique are reported in Table (4). This table shows that, the deep-seated causative bodies (basement rocks) range from 1.44 km at the northwestern part (G16) to about 5.5 km at the main basin (G10).

Table (4): The depths (m) of wells reached the basement.

Gravity profiles	
Profile no.	Depth to basement (m)
G1	2839
G2	2665
G3	3892
G4	3915
G5	3584
G6	2714
G7	4274

G8	3222
G9	3942
G10	5477
G11	4116
G12	2976
G13	3997
G14	1981
G15	4927
G16	1444
G17	3813
G18	2194
G19	2770
G20	3634

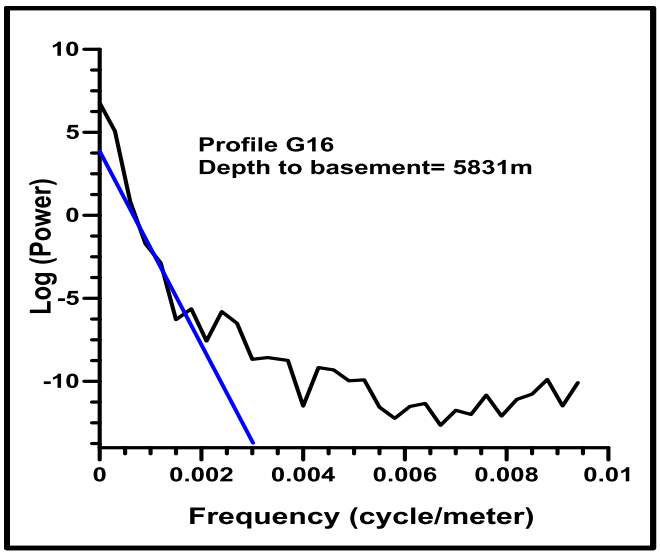

Figure Error! No text of specified style in document.Error! No text of specified style in document.**(11):** Spectral analysis technique along gravity profile (G16).

The tilt angle derivative (TDR)

The TDR technique is used mainly to locate the edges of magnetic and gravity sources. It is a new technique for the interpretation of gridded magnetic and gravity data based on the arctan of the vertical derivative divided by the total derivative. In all cases, the TDR estimates the source parameters with suitable precision. Because TDR utilizes second order derivatives of the gravity or magnetic anomaly, it is quiet sensitive to noise in the data.

Figure (12) shows the application of TDR technique on the high-pass filtered map. The figure reveals the edges of the geologic features such as faults. It facilitates the horizontal locations with extent of edges. It is suggested that the zero-contour line (the solid black line) in the TDR map is the location of unexpected changes in the rock density between positive and negative anomalies that are characterized by sharp gradient. Therefore, the zero-contour line represents the contact boundary of gravity sources. The Zero value (black line) separates the negative values and positive values (Figure 12). On other hand, positive values are situated above the gravity sources (uplifted blocks and/or intrusions) while negative ones are found away from these sources. The TDR of gravity field data shows a NW lineament trend along northwestern part of the study area with large corresponding features along the GS.

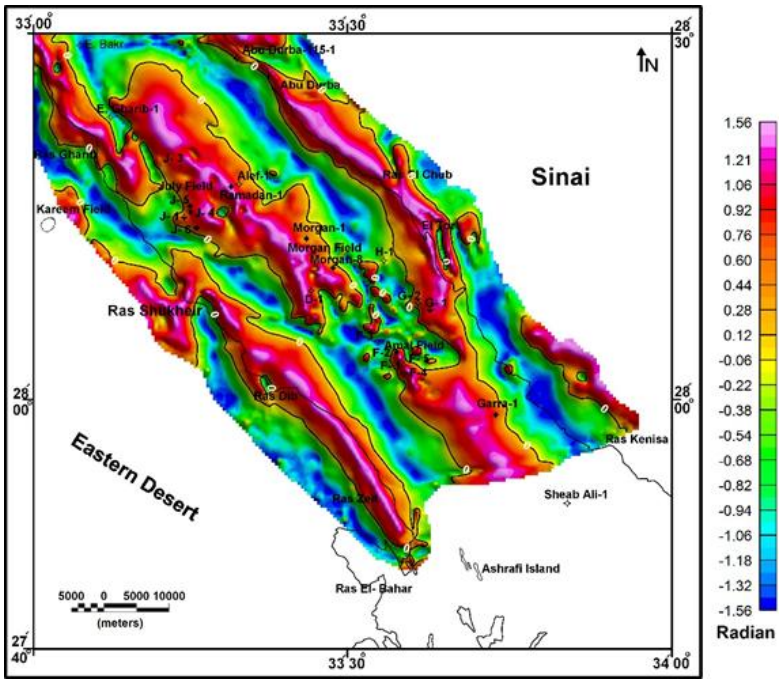

Figure (12): Shaded map shows the TDR of the high pass gravity data. The black line shows the 0 contour of the TDR.

Tentative structural basement maps

The structural map is constructed from the integration of all previous analytical techniques applied to gravity data within the study area. Therefore, this map exposes the structural pattern of the basement rocks as deduced from gravity data as illustrated in Figure 13. The map illustrates parallel uplifted and down-faulted blocks trending mainly in the NW direction. Four transform faults intersect the uplifted and downfaulted blocks taking NNE to ENE direction. Accordingly, the normal faults are predominant and play the main role in the subsurface basement structure within the study area.

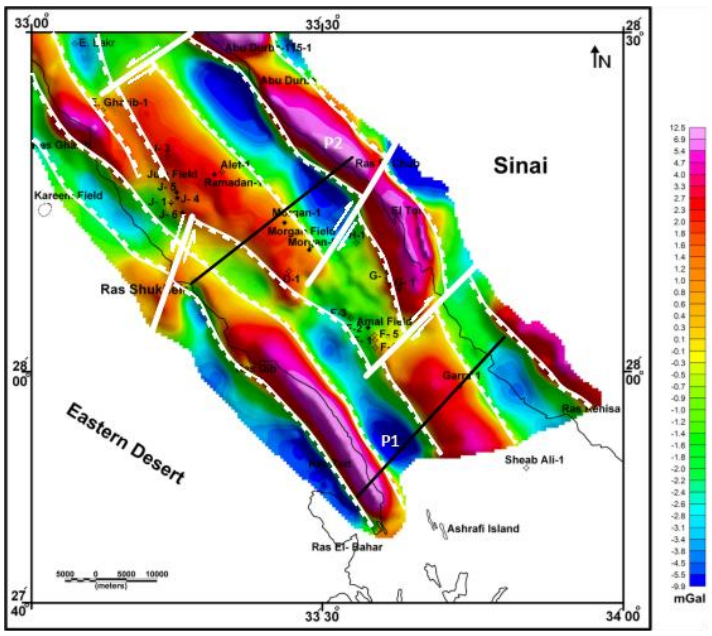

Figure (13): Tentative structure map as deduced from the analysis of gravity data shows the location of the modeling profiles (black lines).

The comparison of the location of the oil producing well (Figure 1) to these constructed maps indicates that nearly all these wells are associated with the uplifted blocks. On the other hand, the location of the dry wells is rarely linked with these uplifted blocks. Tables (5 and 6) indicate the name, the locations (latitudes and longitudes), and the total depth as well as the final formation for both oil and basement wells. In addition, these wells are used to constrain the 2D-gravity models.

Table (5): Oil drilled well within the study area.

Well No.	WELL name	Latitude	Longitude	TD (m)	Fm TD
1	RR 89-2B	27 40 55.300	33 33 58.100	1208	Kareem
2	AS 404 B-1X	27 48 24.700	33 43 01.200	2306	Basement
3	AS 404 D 1-X	27 48 54.500	33 41 55.700	2750	Basement
4	SG 310-4	28 15 11.400	33 13 30.300	3231	Mheiherrat
5	Ashrafi SW-3X	27 46 34.200	33 42 32.100	1905	Basement
6	LL 87-SE-1	28 12 50.900	33 21 09.400	4002	Nubia
7	QQ 89-1	27 44 34.500	33 34 07.300	1219	Granite Wash
8	LL 87-3	28 12 13.700	33 21 22.700	2626	Miocene Rudeis
9	SB 293-2	28 19 40.700	33 15 01.500	4173	Nubia
10	GS 315-3	28 14 18.000	33 28 52.000	3734	Kareem
11	Bdr-C13A	28 14 33.500	33 29 37.700	4304	Kareem
12	GS 356-1(WALI-1)	28 02 38.600	33 36 05.100	3210	Eocene
13	GH 377-1	27 58 19.100	33 47 54.100	1962	Upper Rudeis
14	M 120-208 (DEEP)	28 13 21.600	33 26 56.400	3614	Pre-Miocene
15	E.Zeit 391-3	27 52 34.000	33 41 25.700	3545	Basement
16	E.Zeit 391-4	27 52 10.400	33 41 13.300	3785	Basement
17	SG 300-8	28 18 33.200	33 09 01.200	2101	Nubia C
18	GH 404-1	27 50 12.600	33 43 37.100	3085	Basement
19	GA 84-10M	28 04 00.300	33 23 04.700	1930	Basement
20	AMAL-11	28 03 41.300	33 34 42.100	3050	Miocene
21	RF-A6	28 24 16.140	33 05 04.110	1166	Belayim (Nullipore)
22	RF-B10	28 23 07.161	33 05 12.341	1539	Belayim
23	BM-49 (DIR)	28 27 59.800	33 05 30.800	3370	Nubia
24	GS 323-1 (Sqqara)	28 12 09.770	33 21 40.140	4547	Nubia
25	GS 373-4	27 59 18.911	33 37 37.045	3295	Nubia
26	Ashrafi K-1	27 48 54.521	33 41 55.698	2499	Kareem
27	East Zeit C-5x	27 51 25.792	33 42 34.129	3665	Basement
28	Ashrafi J-1	27 47 10.700	33 42 41.400	1975	Matulla
29	Ashrafi SW-6X	27 46 49.800	33 42 57.500	1936	Basement
30	Ashrafi H-1	27 47 51.320	33 43 22.540	2499	Basement
31	SG 310-7	28 14 24.600	33 14 17.200	3543	Hawara
32	GS 301-1	28 18 27.300	33 13 27.700	4324	Hawara
34	E.Zeit A-21	27 52 34.600	33 41 42.400	4968	Basement
35	GS 302-3	28 17 56.900	33 18 12.700	3993	Nubia

36	Amal-12	28 04 17.000	33 34 18.800	2980	Miocene
37	Amal-10A	28 03 41.200	33 34 42.000	2600	Miocene
38	Bdr-E-1	28 14 04.000	33 26 53.600	3337	Thebes
39	Srm-1A	28 13 52.000	33 21 01.600	3888	Nubia
40	RR 89-1	27 41 55.900	33 34 05.900	757	Basement
41	Sinai-4	28 00 12.200	33 44 21.500	2840	Nubia
42	Sinai-2	28 00 40.200	33 44 14.700	2915	Nubia
43	Shukheir M-2	28 09 51.600	33 16 22.600	3276	Lower Miocene
44	LL 87-2	28 15 46.900	33 19 52.200	3751	Nubia
45	LL 87-5	28 11 38.700	33 22 33.900	3962	Nubia
46	GH 452-1A	27 42 14.400	33 58 37.300	1922	Basement
47	KK 84-2	28 23 49.500	33 05 25.800	823	Belayim
48	KK 84-1	28 23 11.800	33 05 42.500	1604	Nubia
49	GS 325-1A	28 12 22.000	33 26 58.100	3749	Nubia
50	GS 311-1 (J-4)	28 15 44.300	33 15 24.700	3101	Pre Miocene
51	Morgan-1	28 13 39.700	33 26 05.500	3172	Paleozoic
52	Amal-2	28 04 22.000	33 34 10.000	3052	Paleozoic
53	Geisum W-2	27 40 31.700	33 39 22.600	2954	Basal Miocene
54	Alma-4	27 50 03.600	33 52 15.500	2105	Basement
55	Alma-3	27 50 02.900	33 52 16.200	1941	Basement
56	Amal-7	28 04 20.700	33 33 06.500	2827	Senonian Turonian
57	Shoab Gharib-2	28 23 00.800	33 04 26.000	757	Senonian
58	GS 277-1	28 24 43.300	33 18 00.200	4177	Cenomanian
59	Erdma-1	28 11 54.800	33 20 13.600	4109	Cenomanian
60	SB 305-1A	28 18 16.600	33 26 33.800	4085	Nubia
61	GS 315-1(BDR-B1)	28 14 05.600	33 27 53.500	3946	Nubia
62	GS 345-2	28 05 19.300	33 32 20.300	2621	Miocene Rudeis
63	GS 346-1	28 05 32.100	33 33 34.200	3034	Lower Senonian
64	Amal-10	28 03 41.200	33 34 42.000	2600	Miocene Rudeis
65	Amal-8	28 03 24.100	33 34 59.900	2901	Cenomanian
66	GS 381-1	27 56 26.500	33 38 32.400	3541	Nubia
67	SB 339-1A	28 07 55.900	33 38 46.000	1878	Nubia
68	SB 367-1A	28 01 34.000	33 43 30.800	3418	Lower Senonian
69	GH 375-1	27 56 35.900	33 44 56.300	3841	Basement
70	GH 385-1	27 55 56.300	33 49 25.300	2514	Senonian Turonian
71	SRM-2	28 14 27.800	33 20 46.900	3874	Cenomanian
72	GS 373-2	27 59 10.300	33 37 34.300	3411	Nubia
73	Amal-9	28 03 41.200	33 34 42.000	3130	Nubia
74	EGJ-1	28 19 15.200	33 13 27.800	3749	Nubia
75	Shukheir Bay-2	28 09 07.800	33 14 20.100	2535	Rudeis

76	Shukheir Bay-1	28 08 27.500	33 14 46.700	2208	Rudeis
77	GS 336-1(NSM-1A)	28 08 44.900	33 31 39.700	2909	Upper Rudeis
78	GS 327-2	28 12 12.500	33 34 26.800	2600	Nubia
79	SB 374-1B	27 56 25.100	33 38 31.700	3719	Nubia
80	Ghara M-1	27 59 14.600	33 43 46.200	3371	Paleozoic
81	GH 383-1B	27 56 19.200	33 44 13.900	3673	Basement
82	GH 376-1	27 56 35.800	33 44 55.800	3621	Basement
83	GM BA-1(SINAI-1)	28 00 47.800	33 44 58.900	3361	Basement
84	YNS-1 (GS 347-1)	28 07 26.700	33 38 10.100	1965	Basement
85	GS 306-1	28 17 20.000	33 28 08.900	2601	Nubia
86	QQ 89-2	27 43 39.300	33 34 04.500	1549	Basement
87	SB 294-2	28 18 35.100	33 18 19.200	4017	Nubia C
88	SG 300-1A	28 18 34.600	33 09 00.400	2020	Nubia
89	GS 303-1	28 17 31.000	33 18 52.000	3762	Nubia
90	GS 365-1	27 59 40.400	33 37 25.700	3170	Nubia
91	SDK-1	27 56 26.500	33 38 31.700	3407	Nubia
92	SB 374-2C	27 56 26.500	33 38 32.400	3452	Basement
93	GS 391-1	27 52 59.900	33 41 04.900	3658	Nubia
94	J-1	28 15 26.700	33 14 49.800	3278	Paleozoic
95	Sinai N-1	28 00 40.200	33 44 14.500	2395	Rudeis
96	SG 310-6,6A	28 15 04.800	33 12 57.300	4462	Hawara

Two-Dimensional modeling:

To provide additional information about the deep structures of the crust and upper mantle as well as to throw more lights on the geometry and evolution of the study area; two-dimensional modeling is carried out. The gravity data were integrated with offshore geological, geophysical data and two-dimensional (2-D)gravity modeling to reveal the structural configuration of the crystalline basement rocks of the study area [20]**.** Modeling is usually performed by comparing the calculated model anomalies with the observed one, resulting from the field measurements.

According to [21-22] and others, modeling technique comprises two routines Forward and Inverse Modeling approaches which are based mainly on Talwani et al. [23] and Least squares algorithms Abdelrahman et al., [24]**.** The difference between the inverse and forward modeling is, in case of the inverse modeling, an initial deduction for simple model type and employing linear or nonlinear inversion (density, susceptibility, location, and shape and depth inversion) of the observed data into body parameters. While in the forward or iterative modeling, the data linear or nonlinear, inversion is substituted by building and rough estimation of the initial model. Generally, Gravity data depend mainly on the crustal structure, density (composition), and surface elevation. For regional scale, Bouguer anomalies may be suitably clear to give evidence of changes in mass discontinuities in the crust and upper-mantle, as well as the distribution of isostatic balance**.** Recent studies indicate that, the Bouguer anomalies and surface relief are closely connected in general with the crustal thickness [25-28].

The first modeled profile (P1) runs in the NE direction (Figure 14). It was constrained by four wells (Shukeir M-, LL87-5, GS 306-2, and SB 307-1). It passes through the lowest gravity anomaly in the middle part of the study area (-14 mGal) and increases to the East to about (+5 mGal). The minimum depth to the basement surface is 1300 m in the Lower Miocene sediments. The basement rocks were modeled by five polygons forming alternative uplifted and down-faulted blocks. Generally, the modeled section is completely matched with the constructed structural map (Figure 13).

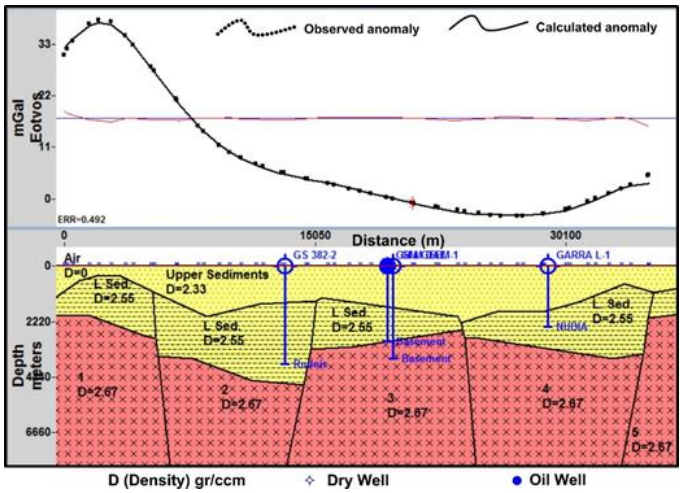

Figure (14): 2D- gravity model along profile P1.

The Second modeled profile (P2) runs in the NE direction (Figure 15). It was constrained by four wells (GS 382-2, GH M Dal, GM Geem-1, and Garra L-1). It passes through the lowest gravity anomaly in the southern part of the study area (-10 mGal) and increases to the north to about (+38 mGal). Generally, gravity profile shows positive anomaly on the western portion then decrease eastward.

In the modeled section, the sedimentary section is represented by two upper (Post Miocene) and lower (Miocene and Pre-Miocene) parts with rock densities of 2.33 and 2.55 g/ccm, respectively. The sedimentary section has two large thicknesses values at the two down-faulted blocks at the western and the eastern parts. The profile crosses alternative down-faulted and uplifted blocks as shown in Figures (15). The basement rocks were modeled by five polygons forming alternative uplifted and down-faulted blocks. The minimum depth to the basement surface is around 2200 m in western and eastern sides. The rock densities of the modeled blocks show granitic rocks of the stanered crustal rocks of 2.67 g/ccm.

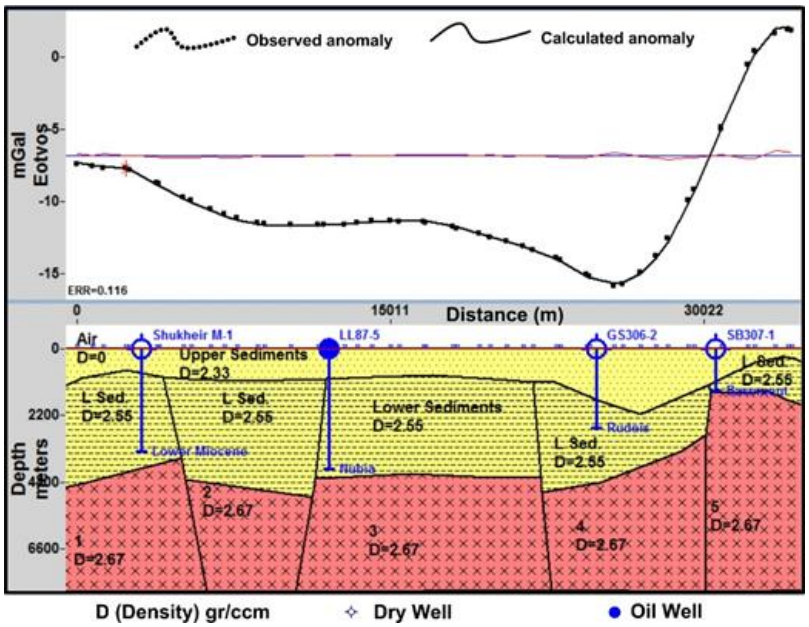

Figure (15): 2.5D gravity model along profile P2.

Basement relief map

A basement relief map is constructed using the average depths estimated from spectral analysis technique (20 profiles) in addition to 84 wells (Table: 6) reached to the basement are used to construct a basement configuration map of the study area (Figure 16). It shows that, the depths to the basement rocks range from 1300 m in the coastal margins in both sides as denoted by the red color to more than 6000 m inside the basin of the northern part between Ras Shukeir and Ras Zeit.

Table (6) and the location of the profiles on Figure (10) show that the depths deduced from gravity data to basement rocks increases toward the middle part of the gulf. It ranges from about 1981m in the northeastern corner (G14) to reaches its maximum value of more than 4972 km (G15). The calculated depths can give an idea about the thickness of the sedimentary succession and the configuration of the sedimentary basins in the study area.

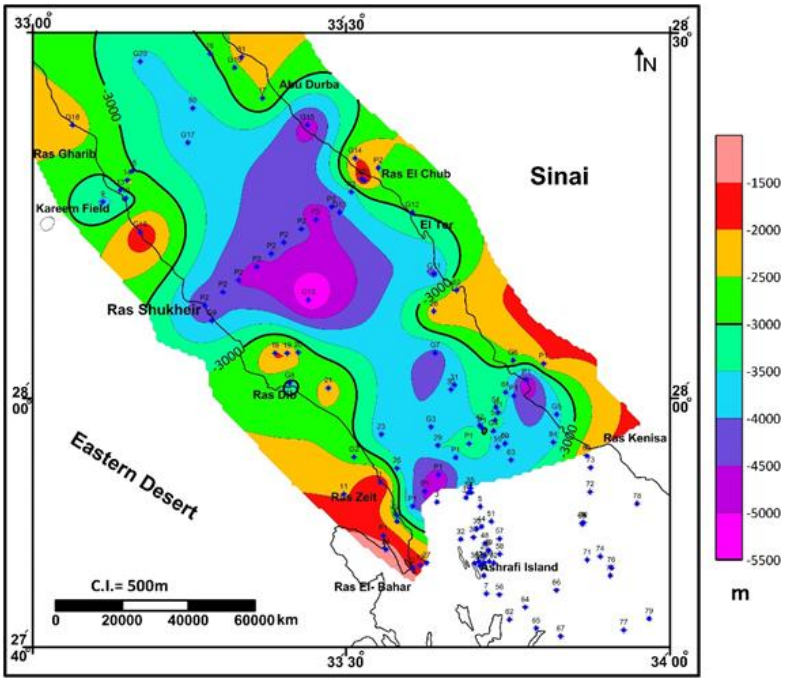

Figure (16): The basement relief map of the study area.

Table (6): The basement drilled wells within the study area.

well No.	WELL	Latitude	Longitude	TD (m)	FMTD
1	W. RAS EL USH-1	27 53 25.990	33 33 05.250	1455	Basement
2	GHANIM-1	27 46 22.708	33 36 11.116	1590	Basement
3	W.ASHRAFI S-1	27 51 47.550	33 38 27.890	4500	Basement
4	E.Zeit A-21	27 52 34.600	33 41 42.400	4968	Basement
5	East Zeit C-5x	27 51 25.792	33 42 34.129	3665	Basement
6	ASHRAFI SW-6X	27 46 49.800	33 42 57.500	1936	Basement
7	NE Geisum-1L	27 44 18.000	33 43 09.300	1615	Basement
8	ASHRAFI H-1	27 47 51.320	33 43 22.540	2499	Basement
9	EL KHALIGUE-1	28 16 24.800	33 06 41.700	3625	Basement
10	S.GHARIB 120-2	28 16 42.100	33 08 53.500	3349	Basement
11	GAZWARINA-1	27 52 26.100	33 29 36.000	2043	Basement
12	EAST RANIM-2	27 46 36.200	33 36 50.700	1684	Basement
13	SG SW-1	28 17 22.400	33 08 21.500	3267	Basement
14	S.GHARIB M-1	28 18 11.000	33 09 01.000	2290	Basement
15	SG 300-4	28 18 56.400	33 09 30.500	2984	Basement
16	SB 268-2	28 28 33.900	33 16 52.300	3020	Basement
17	GS 278-1	28 24 54.500	33 21 52.800	2489	Basement
18	GA 84-10M	28 04 00.300	33 23 04.700	1930	Basement

19	GS 352-1	28 04 00.000	33 24 13.500	2015	Basement
20	ESO 352-2A	28 04 04.000	33 25 16.000	2587	Basement
21	NN 88-1	28 01 09.000	33 28 08.400	2205	Basement
22	SB 307-1	28 18 17.900	33 31 18.300	1373	Basement
23	ERDMA-2	27 57 21.100	33 33 10.100	3836	Basement
24	QQ 89-11	27 47 55.400	33 33 36.600	1130	Basement
25	OO 89-1	27 54 34.300	33 34 39.300	3437	Basement
26	QQ 89-10	27 46 24.900	33 35 .	1252	Basement
27	E.RANIM	27 46 49.100	33 37 28.400	2002	Basement
28	YNS-1 (GS 347-1)	28 07 26.700	33 38 10.100	1965	Basement
29	SB 374-2C	27 56 26.500	33 38 32.400	3452	Basement
30	Ga 87-4	28 01 01.100	33 39 47.800	3790	Basement
31	SB 366-1	28 01 24.100	33 40 06.600	3692	Basement
32	AS 403-1X	27 48 44.700	33 40 43.000	2503	Basement
33	E.ZEIT 391-4	27 52 10.400	33 41 13.300	3785	Basement
34	E.ZEIT 391-3	27 52 34.000	33 41 25.700	3545	Basement
35	GS 392-2	27 52 56.200	33 41 38.600	3664	Basement
36	ASHRAFI D-3X	27 48 54.500	33 41 55.700	2981	Basement
37	AS 404 D 1-X	27 48 54.500	33 41 55.700	2750	Basement
38	W.ASHRAFI-1	27 46 47.000	33 42 03.000	2049	Basement
39	AS 404-1X	27 49 36.600	33 42 15.600	3612	Basement
40	ASHRAFI SW-1X	27 46 55.300	33 42 25.900	1695	Basement
41	ASHRAFI SW-4X	27 46 55.300	33 42 26.100	1951	Basement
42	GM GEEM-1	27 58 07.500	33 42 31.700	3689	Basement
43	ASHRAFI SW-3X	27 46 34.200	33 42 32.100	1905	Basement
44	ASHRAFI N-1	27 49 47.700	33 42 41.800	3698	Basement
45	ASHRAFI SW-2X	27 46 41.500	33 42 48.400	2017	Basement
46	S. ASHRAFI-1B	27 45 46.300	33 42 55.600	2063	Basement
47	AS 404 C-1X	27 47 25.400	33 42 58.900	1970	Basement
48	AS 404 B-1X	27 48 24.700	33 43 01.200	2306	Basement
49	AS 404 B-2X	27 47 51.400	33 43 22.400	1799	Basement
50	E.ASRAFI-1	27 46 56.000	33 43 25.000	3657	Basement
51	GH 404-1	27 50 12.600	33 43 37.100	3085	Basement
52	AS 404 B-3X	27 46 48.200	33 43 51.600	2169	Basement
53	GH M DAL	27 58 30.600	33 43 58.900	3000	Basement
54	GARRA M-4A	27 59 33.800	33 44 03.000	3072	Basement
55	GH 383-1B	27 56 19.200	33 44 13.900	3673	Basement
56	FH 88-9M	27 44 12.200	33 44 24.100	2086	Basement
57	GH 418-1A	27 48 47.000	33 44 25.000	3011	Basement
58	AS 418-1X	27 47 32.100	33 44 25.600	2364	Basement
59	GH 376-1	27 56 35.800	33 44 55.800	3621	Basement
60	GH 375-1	27 56 35.900	33 44 56.300	3841	Basement

61	GM BA-1(SINAI-1)	28 00 47.800	33 44 58.900	3361	Basement
62	GEISUM E-1	27 42 10.400	33 45 21.400	940	Basement
63	GMA-1	27 55 14.500	33 45 30.600	3697	Basement
64	GUBAL N-1	27 43 10.500	33 46 50.600	2079	Basement
65	E GEISUM-2	27 41 27.300	33 47 53.700	1368	Basement
66	GH 434-1C	27 44 34.200	33 49 49.500	4182	Basement
67	GUBAL E-1	27 40 48.000	33 50 13.500	2608	Basement
68	ALMA-4	27 50 03.600	33 52 15.500	2105	Basement
69	ALMA-3	27 50 02.900	33 52 16.200	1941	Basement
70	ALMA-2	27 50 06.500	33 52 23.600	2062	Basement
71	SEGOS-1	27 47 03.940	33 52 45.100	2716	Basement
72	GH 395-1	27 52 37.700	33 53 01.500	2178	Basement
73	GH 386-1A	27 54 37.200	33 53 04.000	2046	Basement
74	GH 420-1	27 47 20.900	33 53 59.800	3003	Basement
75	SEGOS-2	27 45 46.500	33 54 56.000	2290	Basement
76	GH 421-1	27 46 26.000	33 55 01.800	2385	Basement
77	GH 451-1B	27 41 17.800	33 56 13.100	2798	Basement
78	GH 397-1	27 51 40.700	33 57 29.400	2055	Basement
79	GH 452-1A	27 42 14.400	33 58 37.300	1922	Basement
80	BELAYIM BAY-1	28 24 05.400	33 15 14.800	3607	Basement
81	ABU DURBA 115-1	28 28 17.000	33 19 53.700	2092	Basement
82	YORAM-1	28 09 10.000	33 40 20.000	2177	Basement
83	YAEL-2	27 55 36.000	33 52 42.000	1913	Basement
84	GH 375-2	27 56 43.000	33 49 30.300	3552	Basement

IV. Conclusion

From the present study, we can conclude that trend analysis on the gravity data, indicates that, the area is affected by Suez (N 35º-45ºW), East African (N-S), Aqaba (N15º- 25ºE), Najd (N55º-65ºW) trends and Tethyan (E-W) as arranged in a decreasing order. The regional - residual separation is applied to the Bouguer gravity map to separate and focus on the shallow anomalies (structures). The residual gravity maps indicate that, there are new negative and positive anomalies with increasing depth within the GS and the studied area can be considered as large main basin. The northern part of the basin is located inside the northern offshore part. The depths to the basement rocks are calculated along twenty gravity profiles covering almost the study area using the spectral analysis technique. The depth to basement varies from 1300m to exceed 6000m in the middle part. A basement relief map is constructed using the average depths estimated from the spectral analysis technique (22 profiles), as well as 16 basement wells, in addition to 70 wells their total depths are in the Nubia facies, where a 300 m thickness is summed to their total depths to construct this tentative basement map. It illustrates that, the depths to basement are varied from one place to another. At both sides of the gulf, it ranges from 1.2 km to 3km. While inside the gulf basin, the depth increases toward the middle parts, it ranges from 3km to about 5.5 km in the central parts. A basement structural map is constructed using the integrations of all the results obtained from the previous analytical and interpretation techniques on the gravity data. It shows alternative highs and lows parallel to the GS shoreline formed by normal faults trending in the NW-SE direction. These highs and lows are intersected by transform faults of left and right-lateral components. A forward 2D-gravity modeling is applied to provide additional information about the deep structures and to throw more lights on the geometry and evolution of the study area.

Finally, the study indicates that the area contains promising sites for the hydrocarbon accumulations, where it contains different geological structures and great thickness of sediments. Consequently, it is recommended to carry out more perspective work in the study area, especially in the northern offshore part. Also, deep drilling must be carried out within the expected sedimentary basins (promising sites), which have depths of basement of about 5.5 km.

References

[1]. Mckenzie, O.P. and Daves, P., 1970: Plate tectonics of the Red Sea and East Africa, Nature, Vol. 22, pp. 243 - 248.
[2]. Said, R., 1962: The Geology of Egypt. Elsevier Publ. Co., Amsterdam. Oxford and New York, pp. 377.
[3]. Sultan, N. and Schutz, K., 1984: Cross faults in the Gulf of Suez area. EGPC, 7th Explor. Semin., Cairo, pp. 1-15.
[4]. Darwish, M., El-Araby, A., 1993: Petrography and diagenetic aspects of some siliclastic hydrocarbon reservoir in relation to the rifting of the Gulf of Suez, Egypt. Geol. Soc. Egypt., Spec. Publ., No. 1: 155-187.
[5]. Moustafa, A. M., 1976: Block faulting in the Gulf of Suez EGPC., 5th Explor. Semin. Cairo, pp. 19.
[6]. Moustafa, A. M., 1992: Rifting under sediment loading in the Gulf of Suez, Egypt. 11th Petrol Explor. Proj. Co., Cairo, Vol. 1, pp. 1-15.
[7]. Colletta, B., Le Qelle, P. Letouzey, I. and Moretti, L.I., 1988: Longitudinal evaluation of the Suez rift structure. Egypt. Tectonophys., Vol. 153, pp. 221-233.
[8]. Van der Ploeg, P., 1953: Egypt, in: V.C. Illing, the world's oil fields; The Eastern Hemisphere. Sci. Petrol., Oxford, Univ. Press, London, England. Vol. 6, Part 1, pp. 151-157.
[9]. Abdel Gawad, M., 1970: The Gulf of Suez, a brief review of Stratigraphy and structure. Phil. Trans. Roy. Soc. Lond. A. 267, pp. 23-40.
[10]. Meshref, W.M., Refai, E.M. and Abdel Baki, S.M., 1976: Structural interpretation of the Gulf of Suez and its oil potentialities. EGPC., 5th Petrol Explor. Semin., Cairo. pp. 21.
[11]. Shaaban, M.A., 1984: Relief and structures of basement rocks, as deduced from gravity data, In the Gulf of Suez and Sinai Peninsula. Fac. Sci. Bull., Zag. Univ. pp. 11.
[12]. Egyptian General Petroleum Company, stratigraphic committee Oligocene and Miocene Rock-Stratigraphy of the Gulf of Suez Region (EGPC, 1964).
[13]. Nettleton, L.L. 1976: Gravity and magnetic in oil exploration. Mc. Graw. Hill Publ. Co., New York, pp. 464.
[14]. Roy, A., 1966: The method of continuation in mining geophysical interpretation. Geoexploration, 3, pp. 65.
[15]. Arora, K., Cazenave, A., Engdahl, E., Kind, R., & Manglik, A. 2011: Encyclopedia of solid earth geophysics.
[16]. Spector, A., and Grant, F. S., 1970: Statistical models for interpreting aeromagnetic data. Geophysics, 35, 293–302.
[17]. Affleck, L., 1963: Magnetic anomaly trend and spacing patterns. Geophys., Vol. 28, pp. 379-395.
[18]. Assaad, F. A., LaMoreaux, P. E., Assaad, F. A., & LaMoreaux, P. E. 2004: Surface Geophysical Exploration Methods. In Field Methods for Geologists and Hydrogeologists. Springer Berlin Heidelberg.
[19]. Cai, H. (2015): advanced methods for depth-to-basement estimation using gravity, magnetic, and electromagnetic data.
[20]. Lenhart, A., A-L Jackson, C., Bell, R. E., Duffy, O. B., Gawthorpe, R. L., & Fossen, H. 2019: Structural architecture and composition of crystalline basement offshore west Norway." Lithosphere 1. Geological Society of America lithosphere, 11(2), pp. 273–293.
[21]. Reeves, C. V., & MacLeod, I. N. 1983: Modelling of Potential Field Anomalies - Some Applications for the Microcomputer. First Break, 1(8).
[22]. Paterson, N. R., & Reeves, C. V. 1985: Applications of gravity and magnetic surveys: the state of the art in 1985. Geophys., 50(12), pp. 2558–2594.
[23]. Talwani, M., Worzel, J. L., & Landisman, M. 1959: Rapid gravity computations for two-dimensional bodies with application to the Mendocino submarine fracture zone. Journal of Geophysical Research, 64(1), pp. 49–59.
[24]. Abdelrahman, E. M., El-Araby, H. M., El-Araby, T. M., & Abo-Ezz, E. R. 2001: Three least-squares minimization approaches to depth, shape, and amplitude coefficient determination from gravity data. Geophys., Vol. 66(4), pp.1105–1109.
[25]. Wollard, G.P., 1959. Crustal structure from gravity and seismic measurements. J. Geoph. Res. 64, 1521–1544.
[26]. Riad, S., Fouad, A., Refai, E. & Ghaleb, M., 1983: Preliminary interpretation of regional gravity anomalies of Egypt. The 8th General Assembly of the IUGG, Hamburg.
[27]. Blasy, M., Baroudy, A.F. and Kharbish, S.M., 2001. Geochemical characteristics of Wadi Tarr albitite, Southeastern Sinai, Egypt. Egypt J Geol, 42, pp.767-780.
[28]. Riad, S. and El-Etr, H.A. 1985: Bouguer anomalies and lithosphere- crustal thickness in Uganda. Journal of Geodynamics, Vol. 3, pp. 169-186.